ACS APPLIED NANO MATERIALS

www.acsanm.org Article

Poly(β-amino ester) Nanoparticles Modified with a Rabies-Virus-Derived Peptide for the Delivery of *ASCL1* across a 3D *In Vitro* Model of the Blood–Brain Barrier

Tina M. Rodgers, Nicolas Muzzio, Andrea Valero, Ikram Ahmad, Tanja Ursula Lüdtke, Sergio E. Moya, and Gabriela Romero*

Cite This: *ACS Appl. Nano Mater.* 2023, 6, 6299–6311 Read Online

ACCESS | Metrics & More | Article Recommendations | Supporting Information

ABSTRACT: Gene editing has emerged as a therapeutic approach to manipulate the genome for killing cancer cells, protecting healthy tissues, and improving immune response to a tumor. The gene editing tool achaete-scute family bHLH transcription factor 1 CRISPR guide RNA (*ASCL1-gRNA*) is known to restore neuronal lineage potential, promote terminal differentiation, and attenuate tumorigenicity in glioblastoma tumors. Here, we fabricated a polymeric nonviral carrier to encapsulate *ASCL1-gRNA* by electrostatic interactions and deliver it into glioblastoma cells across a 3D *in vitro* model of the blood–brain barrier (BBB). To mimic rabies virus (RV) neurotropism, gene-loaded poly(β-amino ester) nanoparticles are surface functionalized with a peptide derivative of rabies virus glycoprotein (RVG29). The capability of the obtained NPs, hereinafter referred to as RV-like NPs, to travel across the BBB, internalize into glioblastoma cells, and deliver *ASCL1-gRNA* is investigated in a 3D BBB *in vitro* model through flow cytometry and CLSM microscopy. The formation of nicotinic acetylcholine receptors in the 3D BBB *in vitro* model is confirmed by immunochemistry. These receptors are known to bind to RVG29. Unlike Lipofectamine which primarily internalizes and transfects endothelial cells, RV-like NPs are capable to travel across the 3D BBB in vitro model, preferentially internalizing glioblastoma cells, and delivering *ASCL1-gRNA* at an efficiency of 10%, causing noncytotoxic effects.

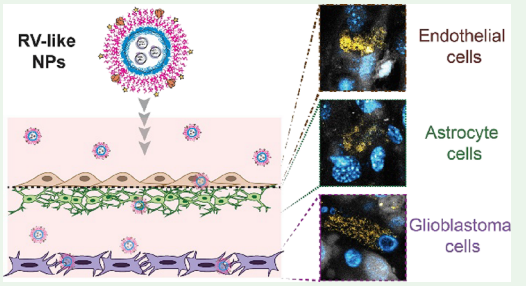

KEYWORDS: *polymer nanoparticles, gene delivery, virus-like nanoparticles, glioblastoma multiforme, blood–brain barrier model*

1. INTRODUCTION

Glioblastoma multiforme (GBM) is the most common, aggressive, and lethal form of brain cancer. GBM is thought to form through communication between tumor-associated reactive astrocytes and glial cells. This connection promotes the aggressiveness and progression, along with the survival, of the tumor.[1] Existing GBM therapies consist of surgical resection with succeeding localized radiation therapy and chemotherapy. All current treatments have limitations. For instance, surgical resection is invasive and normally only performed depending on the tumor's shape, size, and location. Localized radiation is known to cause severe DNA damage resulting in cell apoptosis of surrounding healthy tissues.[2] Chemotherapeutic drugs such as temozolomide, the most utilized drug for GMB, also cause damage to the DNA. Unfortunately, these therapeutic treatments not only target tumor cells but also destroy healthy brain tissues.[2,3] None of these treatments are specific to cell type,[4] and even after all treatments are applied, the survival rate is merely 15 months.[5,6]

The blood–brain barrier (BBB) is the biggest biological challenge to overcome in the development of therapies for the treatment of GBM. This semipermeable membrane is highly selective, limiting the blood-borne particles allowed to cross.[7] The BBB not only averts small molecules from entering but contains transporters that evacuate foreign particles.[8] Molecules and nutrients can cross the BBB through carrier-mediated transport, active transport, passive diffusion, and endocytosis.[8] Chemical and physical approaches have been developed to cross the BBB such as vasoactive therapeutics,[9,10] osmotic pressure,[11−13] and microbubbles.[11] Vasoactive agents such as adenosine, histamine, and bradykinin, among others, are utilized to open the BBB vasculature for a short period, which allows not only for drugs to be delivered into the brain but also for toxins to enter.[14,15] Compounds such as mannitol open the tight junctions in the endothelial cell layer hyperosmotically, allowing large molecules across the BBB by passive diffusion. Because of the nonselective gating, the

Received: February 14, 2023
Accepted: March 23, 2023
Published: March 31, 2023

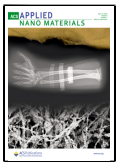

https://doi.org/10.1021/acsanm.3c00651
ACS Appl. Nano Mater. 2023, 6, 6299–6311

uncontrolled inflow of molecules increases the amount of brain fluids, causing aphasia, hemiparesis, and neurological toxicity.[12] Receptor-mediated transcytosis pathways have been explored as a more selective pathway across the BBB. An example of such specific approaches can be found in the use of the rabies virus glycoprotein (RVG)-derived peptides[16,17] for mimicking the rabies virus (RV) transient pathway across the BBB. RVG29 is a 29-residue peptide derived from RVG that binds to the nicotinic acetylcholine receptor (nAchR). RVG29 is being studied as a targeting ligand to cross the BBB and deliver therapeutics to the central nervous system.[18] Using peptides as targeting ligands presents several advantages such as their relatively low molecular weight, easier obtention, relatively low cytotoxicity and immunogenicity, and degradability *in vivo* to naturally occurring compounds.[19]

Gene editing systems have grown as a new approach to treating diseases, including various types of cancer. Gene editing treatments consist of silencing, inserting, replacing, modifying, or deleting parts of the genomic DNA of the tumorous cells.[20] For instance, small interfering RNAs (siRNA) are used as a treatment to silence specific gene(s),[21] whereas meganucleases, zinc finger nucleases (ZFN),[22,23] transcription activator-like effector nucleases (TALENs),[24] clustered regularly interspaced short palindromic repeats (CRISPR/Cas9),[22,24,25] and *piggyBac* transposon/transposase[26] are technologies utilized to modify the genetic makeup by removing and inserting genes.[26,27] Gene editing tools have become important in biological engineering as tunable platforms for precise gene targeting. These therapeutic instruments have the potential to repair the mutations at the genetic level that cause diseases.[25,28] The achaete-scute family bHLH transcription factor 1 CRISPR guide RNA (*ASCL1-gRNA*) gene editing system has been investigated for GBM treatment. ASCL1 reprograms neuronal glioma cells, blocking proliferation[29] through the removal from the cell cycle.[30] ASCL1 is also thought to attenuate tumorigenicity in glioblastoma tumors[31] as well as repair neuronal lineage potential and promote terminal differentiation.[32]

Exogenous plasmids, including the most common gene editing systems, are unable to spontaneously penetrate mammalian cells. Thus, viral vectors are the current delivery system in gene therapies. Viral vectors are effective as they rely on the natural ability of viruses to introduce genetic material into mammalian cells; however, they carry the possibility of immunogenic toxicity and insertional oncogenesis.[33] Moreover, viruses are limited to carrying payloads with sizes between ~4.5 and 5 kb, making them unsuitable for most gene editing systems.[34] Other avenues that have been used for the intracellular delivery of genes utilize physical or chemical manipulations. An example of physical manipulation is electroporation.[35] This technique employs electric shock with high voltage, producing holes in the cell membrane that allow the introduction of genetic material.[36] For chemical manipulation, the most widely adopted technology is the Lipofectamine reagent, a cationic lipid-based system[35,37] and the benchmark for *in vitro* transfection.[38] However, Lipofectamine is highly cytotoxic, limiting its application *in vivo*.[39] Synthetic carriers such as lipids, polymers, or inorganic nanoparticles have been proposed for gene delivery.[40,41] Although synthetic carriers have not been able to match the competence of a virus in terms of transfection efficiency, scientists can utilize materials chemistry and engineering to design them at a low cost, with high reproducibility on a large scale, low immunogenicity,[35,40] and add-on surface recognition functions to overcome biological barriers.

In this work, we have fabricated nanoparticles (NPs) composed of the block copolymer poly(ethylene glycol)-*block*-poly(1,4-butanediol)-diacrylate-*β*-hydroxyamylamine-*block*-poly(ethylene glycol) (PEG-PDHA) for the stable encapsulation and intracellular delivery of the *ASCL1-gRNA* gene editing tool. Chemical cross-linking of PEG-PDHA polymer chains was used for nanoparticle stabilization in physiological conditions following previous investigations from our group on approaches to stabilize PEG-PDHA plasmid nanocarriers.[27] For intercellular nuclear targeting, PEG-PDHA was conjugated with the microtubule associated nuclear localization peptide (MTAS-NLS). PEG-PDHA NPs formed after complexation of the polymer with *ASCL1-gRNA* were surface engineered with RVG29 (RV-like NPs) to mimic the RV biorecognition pathway for crossing the BBB.[16] To assess their therapeutic potential, RV-like NPs fabricated here were investigated using a 3D BBB *in vitro* model. We studied the ability of the NPs to cross the 3D BBB *in vitro* model, penetrating human glioblastoma cells and selectively delivering the *ASCL1-gRNA* editing tool.

2. EXPERIMENTAL SECTION/METHODS

2.1. Materials. 1,4-Butanediol diacrylate, 4-amino-1-butanol, dimethyl sulfoxide (DMSO), triethylamine (TEA), pyridine (Py), sodium chloride (NaCl), poly(ethylenimine) (PEI), sodium hydroxide (NaOH), hydrochloric acid (HCl), Triton, 4′,6-diamidino-2-phenylindole (DAPI), (1-ethyl-3-(3-dimethylaminopropyl)-carbodiimide hydrochloride (EDC), hydroxysuccinimide (NHS), 3-(4,5-dimethylthiazol-2-yl)-2,5-diphynyltetrazolium bromide (MTT), phosphate buffer saline (PBS), fetal bovine serum (FBS), ampicillin sodium salt, and Opti MEM 1 reducing serum media were purchased from Sigma Aldrich. Amine-poly(ethylene glycol)-carboxymethyl (NH2-PEG-COOH) was purchased from Laysan Bio. The endothelial cell growth basal medium (EBM) and endothelial cell growth medium SingleQuots kit was purchased from LONZA. Dulbecco's modified Eagle medium (DMEM), Eagle's minimum essential medium (EMEM), human primary umbilical vein endothelial cell line (HUVEC), Uppsala 87 malignant glioma cell line (U87MG), and immortal mouse clone type I neuronal astrocyte cell line (C8-D1A) were obtained from ATCC. TrypLE Express was purchased from Gibco. UltraPure Agarose, Lipofectamine 3000, LB broth (Miller), SYBR Safe DNA gel stain, and snakeskin dialysis tubing 10 kDa were received from Thermo Fisher Scientific. IgG (H + L) Cross-Adsorbed Goat Anti-Rat, Alexa Fluor 647 secondary antibody, Triton X-100, Sytox Red, and Calcein Green were purchased from Invitrogen. TWEEN-20 was purchased from Fisher Bioreagents. Bovine serum albumin (BSA) was obtained from VWR Life Science. Recombinant anti-nicotinic acetylcholine receptor alpha 1/CHRNA1 antibody was bought from Abcam. Cy5.5 Mono NHS Ester was purchased from Cytiva. The human achaete-scute homolog 1 (ASCL1) enzyme-linked immunosorbent assay (ELISA) kit was purchased from MyBioSource. Tris/borate/EDTA (TBE) buffer was obtained from Alfa Aesar. Plasmid achaete-scute family bHLH transcription factor 1 guide ribonucleic acid (*ASCL1-gRNA*) containing a CMV-puro-t2A-*mCherry* expression cassette was purchased from Addgene as an *Escherichia coli* agar stab. Bacterial amplification was performed using sterile LB broth containing ampicillin and refined utilizing an endotoxin-free DNA purification kit from QIAGEN. The microtubule associated nuclear localization (MTAS-NLS) peptide was purchased from Eurogentec. The 29-residue peptide derived from rabies virus glycoprotein (RVG29) was purchased from GenScript (RP20464). Rhodamine B (RhB) purchased from Chem-Impex Int'l. Inc. Acti-stain 488 phalloidin was obtained from Cytoskeleton Inc. The Millicell ERS-2 volt-ohm

https://doi.org/10.1021/acsanm.3c00651
ACS Appl. Nano Mater. 2023, 6, 6299−6311

meter and 3.0 μm pore size Millicell polyethylene terephthalate hanging cell culture insert were purchased from Millipore Sigma.

2.2. Synthesis of PEG-PDHA. The Michael addition polymerization technique was utilized for synthesizing poly(ethylene glycol)-*block*-poly[(1,4-butanediol)-diacrylate-β-5-hydroxyamylamine]-*block*-poly(ethylene glycol) (PEG-PDHA) as we reported previously.[27,42] Briefly, PDHA was synthesized by mixing 4-amino-1-butanol (7.48 mmol) with 1,4-butanediol diacrylate (8.23 mmol) and heating the mixture to 90 °C for 45.5 h under magnetic stirring and N_2 gas flow. Then, the product was resuspended in DMSO and sonicated with heat. The mixture was centrifuged, and the suspended portion was decanted and dried in a rotary evaporator. The purity of PDHA was verified via proton nuclear magnetic resonance (^{1}H NMR). PDHA was dissolved in DMSO and stored at −20 °C until further needed. Afterward, NH2-PEG-COOH (0.05 mmol) was dissolved in DMSO with pyridine (6.18 mmol) and TEA (3.59 mmol) under magnetic stirring. PDHA was added dropwise to the solution every 12 min at a 1:2 PDHA/NH2-PEG-COOH molar ratio. The reaction was carried out for 24 h to produce COOH terminated PEG-PDHA. PEG-PDHA was purified through dialysis against Millipore water for 2 days. The purity of PEG-PDHA was assessed by ^{1}H NMR. Only the polymer with purity above 80% was utilized in this work. Purified PEG-PDHA was lyophilized and stored at −20 °C.

2.3. PEG-PDHA Functionalization. MTAS-NLS was conjugated to the end-chain of the PEG block from PEG-PDHA. The conjugation occurred through carbodiimide chemistry between COOH end-groups of PEG-PDHA and the amine groups from residual lysine in MTAS-NLS. First, carboxylic groups were activated by suspending 0.006 mmol of PEG-PDHA in 3 mL of 10 mM 1-ethyl-3-(3-dimethylaminopropyl)carbodiimide hydrochloride (EDC) and 10 mM *N*-hydroxysuccinimide (NHS). The suspension was sonicated for dispersion. Activation was carried out on an orbital shaker at 24 °C for 1 h. Then, the pH was adjusted to 8.6, MTAS-NLS (2 nmol) was added, and the suspension was mixed in an orbital shaker at 4 °C for 2 days. The obtained suspension was purified by dialysis against Millipore water utilizing a 10 kDa membrane. Finally, the PEG-PDHA conjugated MTAS-NLS polymer was lyophilized, and purity was verified by ^{1}H NMR.

2.4. Characterization of PEG-PDHA Nanoparticles. The zeta potential and hydrodynamic diameter were measured by dynamic light scattering (DLS) utilizing a NanoSizer (Malvern Nanosize, U.K.). DLS measurements were performed using PBS at 25 °C and at a cell drive voltage of 30 V utilizing the monomodal analysis model. Transmission electron microscopy (TEM) was performed utilizing a JOEL JEM-2010F high-resolution transmission electron microscope at 150 kV to further characterize the particles for size and morphology. Samples for TEM were stained with uranyl acetate prior to imaging.

2.5. Plasmid Encapsulation and Cross-Linking. PEG-PDHA NPs were prepared by mixing bare PEG-PDHA with 10% weight of MTAS-NLS conjugated PEG-PDHA in 0.15 M NaCl above the critical micelle concentration of PEG-PDHA ($CMC_{PEG\text{-}PDHA}$ = 0.015 mg mL^{-1}).[27] *ASCL1-gRNA* plasmid was added carefully at a polymer/plasmid molar ratio of 0.36 for complexation. Encapsulation through complexation was carried out on an orbital shaker at 4 °C for 1 h. Then, 1 mL of a 10 mM EDC/NHS solution was added to the nanoformulation, and the sample was mixed on the orbital shaker at 4 °C for 1 h. Afterward, the pH was adjusted to 8.6 and left overnight on the orbital shaker for cross-linking. After, the sample was centrifuged at 18,000 rpm for 5 min at 4 °C. The supernatant was discarded, and PBS was added to resuspend the pellet. The nanoformulation was placed on an orbital shaker at 4 °C until needed. Plasmid encapsulation was confirmed by 1% agarose gel electrophoresis using TBE as the running buffer. Gel imaging was performed using a Lonza FlashGel Imaging unit and SYBR Safe for plasmid staining. UV-spectroscopy (Nanodrop One^C) was performed to quantify plasmid encapsulation.

2.6. Surface Modification of PEG-PDHA NPs with RVG29. The cross-linked PEG-PDHA nanoformulation was modified via electrostatic interactions to embed RVG29 on the surface. RVG29 was added to the nanoformulation in 0.15 M filtered NaCl (pH 4) at a molar ratio of 0.36 PEG-PDHA/RVG29, sonicated until fully dispersed, and placed on the orbital shaker at 4 °C for 3 days. Then, the nanoformulation was centrifuged at 18,000 rpm for 5 min at 4 °C. The supernatant was discarded, and the obtained RV-like PEG-PDHA NPs were resuspended in PBS and placed on the orbital shaker until used.

Quartz crystal microbalance with dissipation (QCM-D) monitoring was performed to confirm the surface chemistry protocol. QCM-D measurements were performed on a QSense Explorer microbalance (Biolin Scientific). A 14 mm diameter silicon dioxide coated quartz crystal with a fundamental frequency of 5 MHz was used as a sensor (QSX 303, Biolin Scientific). First, a baseline of 0.15 M NaCl at pH 7 was recorded. Then, a layer of PEI was assembled on top of the sensor by injecting a solution of 0.5 mg mL^{-1} PEI in 0.15 M NaCl into the system to provide a positive surface for further assembly. A wash with 0.15 M NaCl at pH 7 was performed to remove the excess of PEI. Afterward, 0.5 mg mL^{-1} of PEG-PDHA in 0.15 M NaCl was adsorbed. After 20 min incubation, the excess of PEG-PDHA was removed through a wash with 0.15 M NaCl at pH 7. Then, PEG-PDHA was cross-linked with 10 mM EDC/NHS solution following the same protocol described above for colloidal NPs. Finally, 0.03 nmol of RVG29 was assembled onto the cross-linked PEG-PDHA surface. After 30 min incubation, the QCM-D sensor was washed with 0.15 M NaCl at pH 7. The QCM-D frequency and dissipation were recorded for seven odd overtones (1st−13th). Changes in resonance frequency (ΔF) and dissipation (ΔD) were monitored during all the experiments. The relationship between ΔF and adsorbed mass was calculated using the Sauerbrey equation:[43,44]

$$m_{\mathrm{QCM-D}} = -C\frac{\Delta f_i}{i}$$

with the mass sensitivity constant of the crystal $C = -17.7$ ng cm^{-2} Hz^{-1} and i the overtone number.

The normalized frequency shifts, $\Delta f = \frac{\Delta fi}{i}$, of the average frequency changes were employed to calculate the mass of the polymer and RVG29 adsorbed on the QCM-D quartz sensor. The ratio of dissipation and normalized frequency shifts, $\Delta D_i/(-\Delta F_i/i)$, was smaller than 0.4×10^{-6} Hz^{-1},[45] fulfilling the conditions to use the Sauerbrey equation.[43]

Fluorescence correlation spectroscopy (FCS) was performed to verify that the RVG29 was attached to the surface of RV-like NPs. First, RVG29 was fluorescently labeled with Cy5.5 Mono NHS Ester via carbodiimide chemistry to produce RVG29-Cy5. FCS experiments were carried out utilizing the LSM 880 confocal laser scanning microscope (CLSM) from Carl Zeiss outfitted with the Confocor 3 FCS module. Briefly, the samples were excited with a helium-neon laser with the wavelength 633 nm, and the confocal volume was calibrated with the free dye ATTO-633 at a concentration of 40 nM. The RVG29-Cy5 as well as nonfluorescent PEG-PDHA NPs were dissolved in water containing 4% SDS. First, the peptide was measured to determine the diffusion coefficient by using the fit-model 3D normal diffusion with the fit algorithms simulated annealing/Levenberg−Marquardt and considering one diffusing component. The estimated diffusion coefficient of the peptide was then used for the two-component fitting of the peptide−nanoparticle complex. The formation of the complex was done by adding the peptide to 0.5 mg mL^{-1} of PEG-PDHA NPs followed by incubation at 37 °C for 1 h and agitation of 200 rpm. The measurement of the peptide−nanoparticle complex was done *in situ* in triplicate.

2.7. 3D BBB *In Vitro* Model. An *in vitro* triple co-culture model of the BBB was adopted from refs 46 and 47 where glass cover slides on the bottom of the well of the 24-well plate and Millicell hanging culture inserts were used. Independently, glioblastoma cells were cultured in EMEM culture media supplemented with 10% FBS, astrocyte cells were cultured in DMEM culture media supplemented with 10% FBS, and endothelial cells were cultured in EBM culture media supplemented with growth factors and 10% FBS. All cell lines were maintained at 37 °C in 5% CO_2. When cells reached ∼80%

https://doi.org/10.1021/acsanm.3c00651
ACS Appl. Nano Mater. 2023, 6, 6299−6311

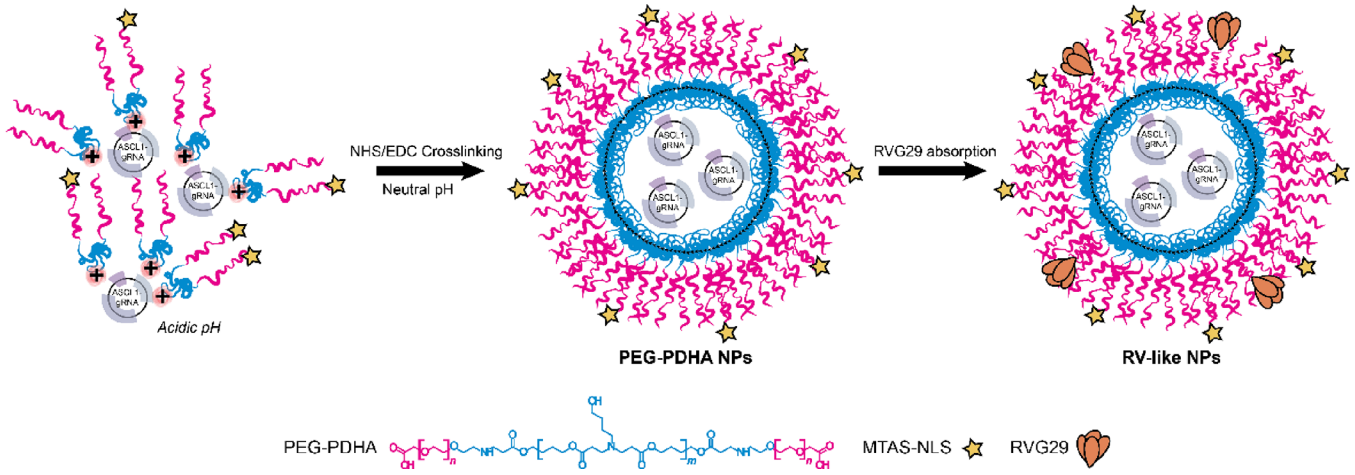

Figure 1. Schematic representation of the fabrication of RV-like nanoparticles encapsulating *ASCL1-gRNA*.

confluency, they were split utilizing TrypLE Express for cell releasing. Glass cover slides on the bottom of wells of the 24-well plate were seeded with 40K of glioblastoma cells. For the Millicell transwell, 60K of astrocyte cells were seeded on the basolateral side of the membrane. After 3 h, the transwell was carefully flipped over, and media were added to the well. After 2 days, 60K of endothelial cells were seeded within the apical chamber of the transwell membrane. After 3 h of co-culturing, media were added to the apical chamber. After 5 days from astrocyte cell seeding, the transwell was hung on the wells of the 24-well plate containing glioblastoma cells in the bottom. The combined co-culture was maintained in both EBM and DMEM culture media supplemented with 10% FBS at 37 °C in 5% CO_2. Half the volume of the culture media was carefully replaced every other day until each cell compartment formed a monolayer.

2.8. Cellular Uptake. For these studies, RV-like NPs were labeled with Rhodamine B isothiocyanate by covalently binding to the carboxylic end groups of PEG.[48] The uptake studies were performed on the 3D BBB *in vitro* model. After cell confluency of 80% and 24 h prior to performing experiments, the media were changed. Prior to the addition of NPs, transendothelial electrical resistance (TEER) was measured to assess the barrier function of the endothelial cells contained on the transmembrane surfaces.[49] Labeled RV-like NPs were added carefully to the middle of the apical chamber of the transwell at plasmid concentrations of 5 $\mu g\ \mu L^{-1}$. Cells were fixed in the transwell and wells at different time intervals, 0, 4, 8, and 12 h with 4% paraformaldehyde solution and permeabilized with 0.1% Triton X-100 for 5 min. Acti-stain 488 phalloidin and DAPI were used for F-actin and nucleus staining, respectively. Every membrane was carefully removed from the support with delicate precision as to not disturb the cells for imaging. A Leica TCS SP8 Confocal Microscope was used to image cells co-cultured with labeled RV-like NPs. Flow cytometry (BD Accuri C6 Plus) was utilized to determine the uptake efficiency of cells co-cultured with labeled RV-like NPs. A fluorescence threshold was set utilizing intact glioblastoma, astrocyte, and endothelial cells. Measurement parameters were set the same for all samples, and each run was set to count 10^4 events. The total percentage of each cell layer containing the fluorescent labeled NPs was determined from the area corresponding to higher intensities than the threshold.

2.9. Transfection Efficiency. The different cell lines were plated in the 3D BBB *in vitro* model as described above. Nonfluorescent RV-like NPs carrying *ASCL1-gRNA* prepared as above were carefully added in 20 μL of Opti-MEM to the wells at concentrations of 5 and 10 $\mu g\ \mu L^{-1}$ of plasmid *ASCL1-gRNA*. RV-like NPs were co-cultured in the 3D BBB *in vitro* model for 2, 3, and 4 days. Lipofectamine 3000 was used as the positive control for transfection efficiency comparison against RV-like NPs. As the *ASCL1-gRNA* plasmid construct contains fluorescent *mCherry*, flow cytometry (BD Accuri C6 Plus) was utilized to quantify the transfection efficiency as a means of *mCherry* protein cell expression. A fluorescence threshold was set utilizing intact glioblastoma, astrocyte, and endothelial cells. Measurement parameters were set the same for all samples, and each run was set to count 10^4 events. The total count of cells that expressed *mCherry* protein was determined from the area corresponding to higher intensities than the threshold. Confocal laser scanning microscopy (CLSM) was utilized to qualitatively characterize *mCherry* protein cell expression using a Leica TCS SP8 Confocal Microscope. ELISA was performed on the 3D BBB *in vitro* model to quantify intracellular *ASCL1* protein concentrations. The cells were plated as stated previously. At 2 and 4 days after RV-like NP addition, media were removed. Transwell membranes were moved to fresh cell-free wells. TrypLE (200 μL) was added to glioblastoma cells on the bottom of the well. TrypLE (200 μL) was also added to the fresh well containing astrocytes attached to the underside of the transmembrane along with 200 μL of TrypLE inside the well with the endothelial cells. After detachment, 500 μL of PBS was used to wash and lift detached cells. Each cell layer was placed in a microcentrifuge tube, and cell lysis was achieved by repeated freeze−thaw cycles. Following steps were performed according to the manufacturer's protocol. Within 10 min of stop solution addition, optical density values at 450 nm were obtained using a plate reader.

2.10. Expression of nAchR in the 3D BBB *In Vitro* Model. RV-like NP specific recognition by the 3D BBB *in vitro* model was evaluated by immunostaining of the anti-nicotinic acetylcholine receptors (nAchR), which bind to RVG29. After fixing and permeabilizing the cells from the 3D *in vitro* model, cells were incubated in a 1% BSA solution for 30 min. Then, BSA solution was removed, and the recombinant anti-nicotinic acetylcholine receptor alpha 1/CHRNA1 antibody was added to the cells. The antibody was incubated for 1 h. Cells were washed three times with 0.05% TWEEN-20 (washing solution) for 5 min each wash to ensure free antibody removal. A solution of the secondary antibody, IgG (H + L) Cross-Adsorbed Goat Anti-Rat conjugated with Alexa Fluor 647, along with Acti-stain 488 phalloidin (for cytoskeleton staining), was added. After 45 min of incubation, samples were washed three times with washing solution. DAPI solution was added for 5 min to all samples to stain the nuclei. Samples were washed again with washing solution, and PBS was added. A Leica TCS SP8 confocal microscope was used for cell imaging.

2.11. Cell Viability. Cell viability was evaluated by a live/dead assay using flow cytometry. Glioblastoma cells were seeded in a 96-well plate at a density of 15K cells per well. Cells were incubated at 37 °C with 5% CO_2 for 24 h to allow adhesion. The samples tested were as follows: naked *ASCL1-gRNA*, empty PEG-PDHA NPs, RV-like NP formulation, and Lipofectamine 3000 carrying *ASCL1-gRNA*. After incubation for 2, 3, and 4 days, TrypLE Express was utilized to detach cells from the 96-well plate surface. Cells were then suspended in

https://doi.org/10.1021/acsanm.3c00651
ACS Appl. Nano Mater. 2023, 6, 6299−6311

FACS solution, and Calcein (live stain) and Sytox (dead stain) were added to the samples right before measuring with the flow cytometer.

2.12. Statistical Analysis. Unless otherwise stated, all experiments were performed in triplicate with data being reported as mean ± standard error. To verify statistical differences, one-way analysis of variance (ANOVA) was performed along with Fisher's least significant difference test for means comparison (p value of 0.05, OriginPro 2016).

3. RESULTS AND DISCUSSION

3.1. Fabrication and Characterization of RV-like NPs. Cross-linked PEG-PDHA NPs were fabricated using MTAS-NLS conjugated and unconjugated PEG-PDHA at a mass concentration of 10% MTAS-NLS-conjugated polymer. The *ASCL1-gRNA* gene editing tool was encapsulated within PEG-PDHA NPs via electrostatic interactions between the negatively charged plasmid and the amine groups of the PDHA block in the polymers that lead to nanoparticle formation. After encapsulation, PEG-PDHA NPs were cross-linked with 10 mM EDC/NHS solution. Then, PEG-PDHA NPs were functionalized with the RVG29 peptide through self-assembly on the NPs' surface to form RV-like NPs (Figure 1).

Transmission electron microscopy (TEM) and dynamic light scattering (DLS) were utilized to characterize the morphology and size of the NPs. TEM images confirmed that bare PEG-PDHA NPs (Figure S1) are spherical in shape with a uniform size distribution and a mean diameter of 8 ± 2 nm. DLS characterization showed that PEG-PDHA NPs (Figure 2b and Figure S1) exhibit a hydrodynamic diameter in the range of 90−250 nm with polydispersity index (PDI) between 0.25 and 0.55. RV-like NPs' morphology and size were also characterized by TEM and DLS. TEM shows that the RV-like NPs also are spherical in shape with a uniform size distribution and mean diameter size of 6 ± 2 nm (Figure 2a). DLS shows that the RV-like NPs had a hydrodynamic diameter in the range of 90−200 nm with PDI between 0.30 and 0.55 (Figure 2b and Figure S1). The NPs' diameter measured by TEM is ∼30× smaller than the hydrodynamic diameter measured by DLS. The size discrepancy between TEM and DLS is expected because the latter is an indirect measurement of the hydrodynamic diameter of PEG-PDHA micelles in a solution, which includes the hydration layer around the particle, whereas the former reflects the morphology size of the dehydrated/collapsed micelles.[50−52] Moreover, the PDI values measured by DLS indicate that the hydrated samples are moderately polydisperse, possibly as a result of NP aggregation in PBS. The surface charge of PEG-PDHA NPs was determined by ζ-potential measurements after each step in the functionalization (Figure 2c). The ζ-potential of unmodified PEG-PDHA NPs is of −5.4 ± 0.1 mV, and when NPs are prepared using 10% of MTAS-NLS conjugated PEG-PDHA, the ζ-potential is −1.8 ± 0.6 mV. In both cases, PEG-PDHA NPs display an almost neutral surface charge as expected from the PEG blocks of the polymer that arrange around the core of the NPs where the nucleic acid is located. At physiological pH, the PDHA block of the co-polymer is not charged; thus, to encapsulate negatively charged plasmid DNA via electrostatic interactions, we first protonated the PDHA block of the co-polymer at pH 4.[27,53−55] After allowing for complexation with *ASCL1-gRNA*, the complex was neutralized to pH 7 to form NPs entrapping *ASCL1-gRNA*. The ζ-potential after encapsulation of *ASCL1-gRNA* at pH 7 changed toward positive values of +6.9 ± 0.7 mV. Encapsulation of the plasmid was also corroborated by gel electrophoresis (Figure 2d). We previously studied the stability of PEG-PDHA NPs as carriers for gene delivery, finding that PEG-PDHA NPs require cross-linking to avoid premature dissociation.[27] Thus, after *ASCL1-gRNA* encapsulation, PEG-PDHA NPs were cross-linked with EDC/NHS, which shifted the ζ-potential toward a negative surface charge of −11.0 ± 0.6 mV. The shift to negative ζ-potential values is indicative of amine groups being cross-linked and comes from free carboxylate end groups of the PEG block. It could also be that in the cross-linked NPs at pH 7, although the plasmid remains trapped within the cross-linked polymer, the plasmid−polymer interaction is weaker; thus, the plasmid is more exposed to the surface, which would also explain the negative charge. Finally, the RVG29 peptide was embedded into the PEG-PDHA nanoformulation through electrostatic interactions to form RV-like NPs. The ζ-potential of RV-like NPs was −25.3 ± 0.3 mV, which suggested the attachment of the negatively charged RVG29 on the surface of the NPs. NPs have an overall net negative charge before RVG29 functionalization. However, we can assume that some regions of the polymer with a positive charge are available for complexation with the negatively charged RVG29.

To corroborate the surface chemistry followed to embed RVG29 onto PEG-PDHA NPs' surface, experiments with the QCM-D were performed (Figure S2). PEG-PDHA was electrostatically deposited on top of a PEI-coated quartz crystal sensor. Then, PEG-PDHA was cross-linked, and RVG29 was assembled on top of the cross-linked polymer. We observed that ∼13 ng cm^{-2} of RVG29 was embedded per 157 ng cm^{-2} of cross-linked PEG-PDHA. To further confirm the attachment of RVG29 to the surface of colloidal cross-linked PEG-PDHA NPs, we performed FCS measurements (Figure S3). RVG29 was chemically bonded to the fluorophore

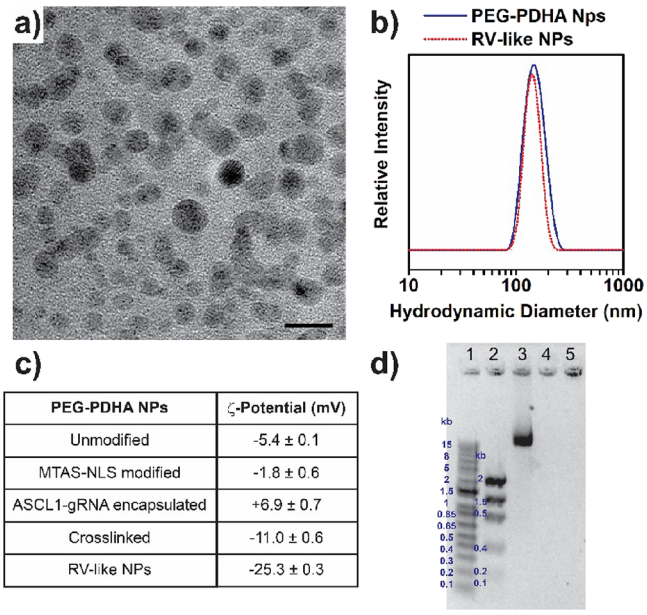

PEG-PDHA NPs	ζ-Potential (mV)
Unmodified	-5.4 ± 0.1
MTAS-NLS modified	-1.8 ± 0.6
ASCL1-gRNA encapsulated	+6.9 ± 0.7
Crosslinked	-11.0 ± 0.6
RV-like NPs	-25.3 ± 0.3

Figure 2. RV-like PEG-PDHA NP characterization. (a) TEM images of RV-like NPs; scale bar = 10 nm. (b) Hydrodynamic size distribution of PEG-PDHA NPs and RV-like NPs. (c) PEG-PDHA NP surface functionalization steps followed by ζ-potential measurements at pH 7. (d) Gel electrophoresis of *ASCL1-gRNA* laden into PEG-PDHA NPs. Well 1: 1 kb plus DNA ladder, well 2: low DNA mass ladder, well 3: *ASCL1-gRNA* (8.3 kb), well 4: PEG-PDHA NPs, and well 5: RV-like NPs.

https://doi.org/10.1021/acsanm.3c00651
ACS Appl. Nano Mater. 2023, 6, 6299−6311

Cy5. FCS allows us to measure the change in the diffusion coefficient of the labeled peptide from a free molecule in bulk to a complex with the NPs. Free RVG-Cy5 had a diffusion coefficient of 73.9 ± 3.0 μm^2 s^{-1}. When RVG29-Cy5 was attached to PEG-PDHA NPs, the diffusion coefficient decreased to 3.3 ± 1.0 μm^2 s^{-1}, indicating that RVG29-Cy5 is no longer freely diffusing but attached to the larger PEG-PDHA NPs.

3.2. Development of a 3D *In Vitro* Model of the BBB. To investigate the potential of RV-like NPs as carriers for gene-editing tools across the BBB, we developed a 3D *in vitro* model of the BBB based on a triple co-culture adapted from Mc Carthy et al.[47] and Stone et al.[46] During the formation process of the 3D BBB *in vitro* model, it is critical to monitor the transendothelial electrical resistance (TEER) and to confirm the formation of tight junctions and barrier functions of epithelial cells on both sides of the porous transmembrane of the transwells.[49] Measurements were carried out at each step in the formation of the 3D BBB *in vitro* model. The TEER (Ω) measurement from the cell-free transwell was subtracted when determining the TEER value of the samples. Moreover, TEER values were multiplied by the surface area of the transwell membrane to obtain the resistance flux (Ω cm^2). A cell-free transwell sample with culture media was used as control. The cell-free transwell displayed a TEER of 18 Ω cm^2. The 3D BBB *in vitro* model was formed by seeding endothelial cells on the apical membrane side representing the endothelial cell layer, astrocyte cells on the basolateral membrane side, and glioblastoma cells in the bottom of the well (Figure 3a).

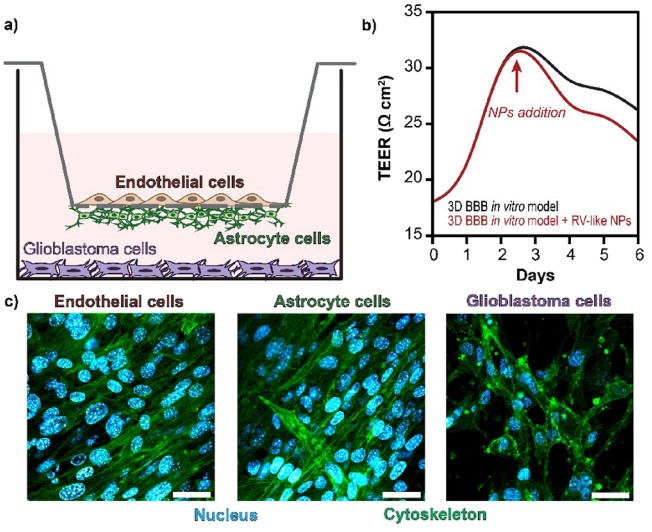

Figure 3. 3D BBB *in vitro* model. (a) Schematic representation of the 3D *in vitro* model of the BBB. (b) TEER monitoring of the 3D BBB *in vitro* model. (c) CLSM images of each cell layer forming the 3D BBB *in vitro* model. Nuclei are stained DAPI (cyan), and cytoskeletons were stained with Acti-stain 488 phalloidin (green). Scale bar = 50 μm.

Physiological TEER values are typically higher than 1500 Ω cm^2;[56] however, 3D BBB *in vitro* models have been reported to display TEER values between 10 and 260 Ω cm^2[46,47,57,58] depending on the pore size and area of the transwell membrane, as well as on the types of cells utilized. It has also been reported that immortalized cells tend to have TEER values lower than 150 Ω cm^2.[56] The formation of the 3D BBB was confirmed by the increase of TEER. Prior to TEER measurements, the electrode was sterilized and equilibrated according to the manufacturer's protocol. TEER measurements started at day 0 as shown in Figure 3b, which displays the TEER changes from the intact 3D BBB *in vitro* model (control) to the exposure to RV-like NPs. The TEER values gradually dropped within 1 day after addition of RV-like NPs on day 2. The decrease in TEER values after nanomaterial addition can be attributed to changes in the cells' tight junctions due to NP exposure[59] and to the cell height increase over time,[49] particularly of glioblastoma cells that tend to form organoid-like structures over time. We further confirm the formation of the 3D BBB *in vitro* model by CLSM imaging of the three different cell layers composing the model (Figure 3c). Through CLSM imaging, it is possible to confirm not only the presence of the three different cell cultures in each layer but also the formation of cell monolayers in each compartment of the transwell (apical and basolateral sides of the transmembrane and the glass coverslip on the bottom of the well) within 6 days. The cell monolayers were very consistent, and overlapping cells were observed in each transwell component of the 3D BBB *in vitro* model.

3.3. Cellular Uptake of RV-like NPs. A necessary component to consider when engineering gene delivery nanocarriers is intercellular uptake. The nanocarrier must be designed to protect the payload from degradation when trafficking the biological system while effectively penetrating and delivering the cargo intercellularly. RV-like NPs fluorescently labeled with Rhodamine B (RhB) were investigated for intercellular uptake across the 3D BBB *in vitro* model. RhB fluorescently labeled NPs were added to the apical chamber of the transwell membrane. All three cell lines were co-cultured with NPs for 4, 8, and 12 h, at which time the well plates were removed, and cells were fixed and stained. CLSM imaging was performed to qualitatively assess NP uptake in the 3D BBB *in vitro* model (Figure 4b,c and Figure S4). Intact cells from each compartment of the 3D BBB *in vitro* model were imaged as control (Figure 4a). PEG-PDHA NPs were tracked in the 3D BBB *in vitro* model after 8 h of co-culturing (Figure 4b). CLSM images show that PEG-PDHA NPs are taken up mainly by endothelial cells. Few PEG-PDHA NPs can cross the endothelial cell layer and be uptaken by astrocytes. No PEG-PDHA NPs were able to travel across the 3D BBB *in vitro* model and internalize glioblastoma cells. When RV-like NPs were added to the 3D BBB *in vitro* model, most of the NPs were found internalized into the astrocyte and glioblastoma cells after 8 h of co-culturing (Figure 4c). This result infers that RV-like NPs are capable to travel through the endothelial and astrocyte cell layers from the transwell to reach glioblastoma cells located in the bottom of the well. Thus, we quantified RV-like NP cell uptake using flow cytometry. Flow cytometry results verified that 99 ± 1% of the endothelial cell layer, 89 ± 3% of the astrocyte cell layer, and 84 ± 4% of the glioblastoma cell layer from the 3D BBB *in vitro* model had taken up RV-like NPs within 8 h of co-culturing (Figure 4d). Cellular uptake was also tracked for PEG-PDHA NPs and RV-like NPs at co-culture times of 4 and 12 h, which showed a similar trend as for 8 h (Figure S4).

3.4. RV-like NPs' Transfection Efficiency in Glioblastoma Cells. The transfection efficiency of the gene editing tool *ASCL1-gRNA* was first investigated in glioblastoma cells using RV-like NPs. The *ASCL1-gRNA* plasmid construct utilized here contains fluorescent *mCherry* coupled within a self-cleaving T2A linker. Thus, transfection efficiency was

https://doi.org/10.1021/acsanm.3c00651
ACS Appl. Nano Mater. 2023, 6, 6299−6311

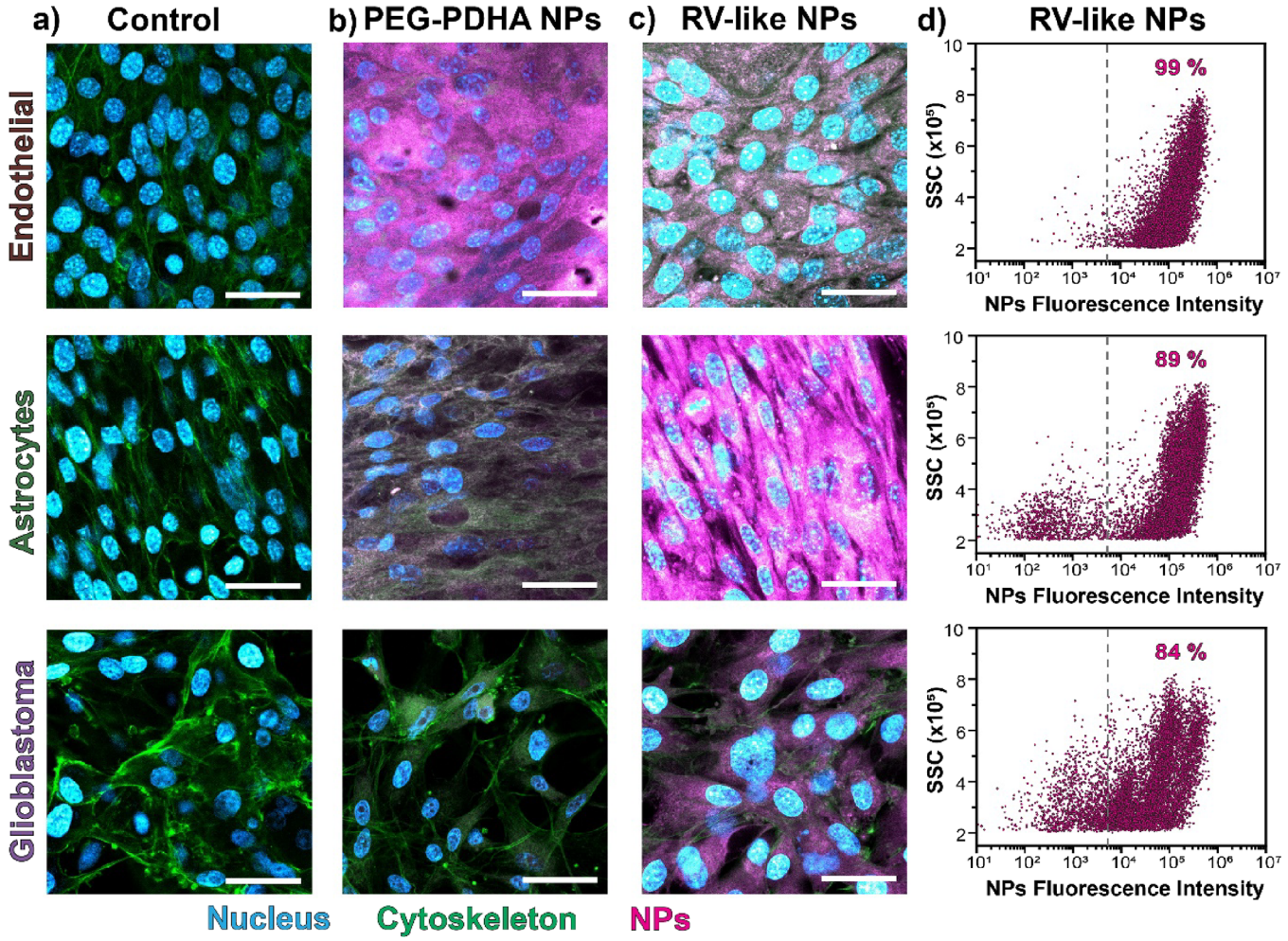

Figure 4. Cellular uptake. CLSM images of each layer composing the 3D BBB *in vitro* model for (a) control (intact cells), (b) cells co-cultured with PEG-PDHA NPs, and (c) cells co-cultured with RV-like NPs. Images were taken after 8 h of co-culturing with the NPs. NPs are labeled with RhB (magenta), cell nuclei are stained by DAPI (cyan), and the cytoskeleton was stained with Acti-stain 488 phalloidin (green). Scale bar = 50 μm. (d) Flow cytometry of cells from each layer of the 3D BBB *in vitro* model exposed to RV-like NPs labeled with RhB for 8 h.

measured by *mCherry* protein expression in cells transfected with *ASCL1-gRNA* through flow cytometry and CLSM. Intact glioblastoma cells were used in this experiment as the negative control to set the fluorescence threshold that will allow for distinguishing *mCherry*-positive from *mCherry*-negative cell populations (Figure 5a,d). Glioblastoma cells transfected with the Lipofectamine 3000 reagent were used as positive control. Transfection with Lipofectamine 3000 resulted in 21.0 ± 1.5% of the glioblastoma cell population expressing *mCherry* protein (Figure 5b,e). Transfection with RV-like NP formulation resulted in 10 ± 1% of glioblastoma cells expressing *mCherry* protein (Figure 5c,f). The transfection efficiency by RV-like NPs is half of what can be achieved when using the commercially available Lipofectamine 3000 reagent. We previously reported the optimization of PEG-PDHA NPs for the encapsulation and intracellular delivery of *PiggyBac* transposon,[27] which yielded a higher transfection efficiency in glioblastoma cells (~55 and ~60% with Lipofectamine 3000). We attribute the lower transfection efficiency of both Lipofectamine 3000 and the RV-like nanoformulation to the cargo size. The *ASCL1-gRNA* plasmid size is 8.3 kbp, whereas *PiggyBac* is only 6.3 kbp. Plasmid size has been identified as a critical factor in transfection efficiency. Previous studies have shown that regardless of the transfection method, large plasmids are more difficult to be delivered into the cells.[60−62] Plasmid size is particularly significant in gene editing therapies, where the therapeutic plasmids required for inserting, modifying, replacing, or deleting parts of the genomic DNA are generally large. Nevertheless, prior research studies have identified the minimum stable transfection efficiency for a successful gene editing therapy to be between 6 and 37%.[63−65]

3.5. RV-like NP Transfection Efficiency across the 3D BBB *In Vitro* Model. Afterward, we evaluated transfection efficiency in the 3D *in vitro* model of the BBB. RV-like NPs were investigated for intercellular delivery of *ASCL1-gRNA* across the three cell layers of the 3D BBB *in vitro* model. The nanoformulation was added to the apical chamber of the transwell membranes. At the co-culturing times of 2, 3, and 4 days, the 3D BBB *in vitro* model was disassembled, and cells were detached for flow cytometry measurements. As previously described, flow cytometry was utilized to quantify transfection efficiency. Intact endothelial, astrocyte, and glioblastoma cells from the 3D BBB *in vitro* model were used as the negative control to set the fluorescence thresholds for cell transfection. For the positive control, we utilized the commercially available Lipofectamine 3000 reagent carrying *ASCL1-gRNA*. After 4 days of co-culturing, the highest transfection efficiency when using Lipofectamine as carrier of *ASCL1-gRNA* was 15.7 ±

https://doi.org/10.1021/acsanm.3c00651
ACS Appl. Nano Mater. 2023, 6, 6299−6311

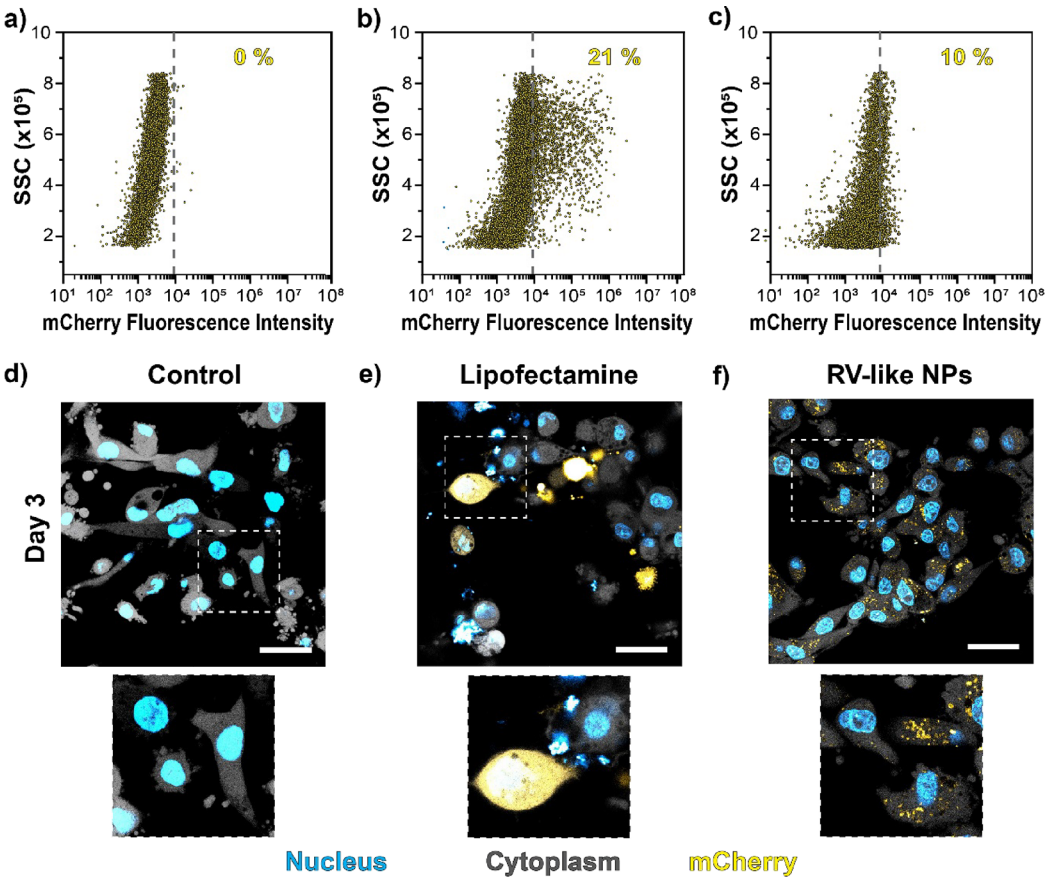

Figure 5. Transfection efficiency into glioblastoma cells. Flow cytometry of glioblastoma cells: (a) intact, (b) transfected with *ASL1-gRNA* using the Lipofectamine reagent, and (c) transfected with *ASCL1-gRNA* using RV-like NPs. CLSM images taken at day 3 post-transfection for (d) control (intact cells), (e) cells transfected with *ASL1-gRNA* using the Lipofectamine reagent, and (f) cells transfected with *ASCL1-gRNA* using RV-like NPs. Nuclei are stained by Hoechst 33342 (cyan), cytoplasm is stained with Calcein (gray), and *ASCL1-gRNA* transfection is visualized by *mCherry* protein (yellow) expression. Scale bar = 50 μm. Enlarged images (2×) of the areas indicated by squares are included.

0.2%, observed in the endothelial cell layer (Figure 6a). Around 8.9 ± 0.8% of transfected astrocyte cells were observed, but the least transfected cells were found to be in the glioblastoma cell compartment (5.8 ± 0.2%). The observed trend indicates that Lipofectamine 3000 transfection efficiency decreases as the cell layers get farther from the administration site. The Lipofectamine 3000 reagent was added to the apical chamber of the transwell that contains endothelial cells. Endothelial cells and astrocytes (basolateral side of the transwell) restrict Lipofectamine traffic across the transmembrane and into glioblastoma cells located at the bottom of the well. When investigating RV-like NPs as carriers of *ASCL1-gRNA*, an opposite trend than Lipofectamine 3000 was observed. At 4 days of co-culturing with RV-like nanoformulation, the highest transfection efficiency was observed in glioblastoma cells with 12.0 ± 2.3% of cells transfected (Figure 6b), indicating that RV-like NPs are capable to pass through the endothelial (2.4 ± 0.2% transfected) and astrocyte (8.8 ± 0.8% transfected) cell layers in the transwell membrane and internalize into glioblastoma cells. *ASCL1-gRNA* transfection efficiencies at days 2 and 3 using Lipofectamine and RV-like NPs are shown in Figures S5 and S6 and are similar to the trends observed at day 4. CLSM imaging was performed to qualitatively assess the intracellular delivery of *ASCL1-gRNA*, which ultimately should result in the cell expression of fluorescent *mCherry* protein. At days 2, 3, and 4 post incubation with Lipofectamine 3000 or RV-like NPs, the 3D cell cultures were removed from the BBB *in vitro* model, and cells were stained with Hoechst 33342 for nuclei labeling and with Calcein green to label the cytoplasm of live cells (Figure 6c−e and Figures S5 and S6). Intact cells were imaged as control (Figure 6c). CLSM imaging confirmed the transfection results measured by flow cytometry. When using Lipofectamine 3000, a higher *mCherry* protein expression is observed in the endothelial and astrocyte cell layers than in glioblastoma cells. On the contrary, RV-like NPs can reach the bottom of the 3D BBB *in vitro* model, internalize into glioblastoma cells, and deliver *ASCL1-gRNA* (Figure 6e) as indicated by *mCherry* protein expression in glioblastoma cells.

Additionally, to assess the quantity of transfection by RV-like NPs, we measured the amount of ASCL1 protein produced by cells using an ELISA. At the co-culturing times of 2 and 4 days, the 3D BBB *in vitro* model was disassembled, and cells were detached utilizing TrypLE. The cells were suspended in PBS, and ASCL1 protein quantification was performed following the ELISA protocol from the manufacturer. Intact cells from the 3D BBB *in vitro* model were used as negative controls. The ASCL1 concentration in the controls was zero as expected because the gene is absent in intact cells. The intracellular ASCL1 protein concentration in all cell lines exposed to RV-like NP formulation increased over time, with higher concentrations observed in glioblastoma cells (Figure 7). On day 2, the ASCL1 protein concentration in glioblastoma cells was ∼450 μg mL^{-1}, increasing to ∼1310 μg mL^{-1} on day 4

https://doi.org/10.1021/acsanm.3c00651
ACS Appl. Nano Mater. 2023, 6, 6299−6311

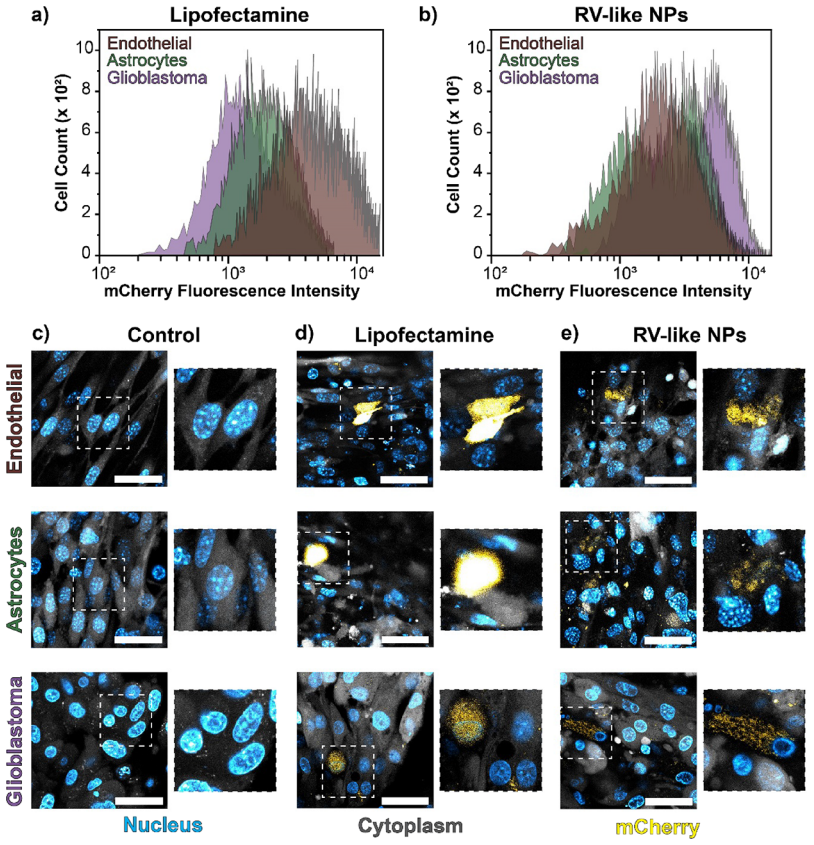

Figure 6. Transfection efficiency across the 3D BBB *in vitro* model. Flow cytometry of cells from the 3D BBB *in vitro* model transfected with *ASL1-gRNA* using (a) the Lipofectamine reagent and (b) RV-like NPs. CLSM images of each layer composing the 3D BBB *in vitro* model for (c) control (intact cells), (d) cells transfected with *ASL1-gRNA* using the Lipofectamine reagent, and (e) cells transfected with *ASCL1-gRNA* using RV-like NPs. Flow cytometry and CLSM images were taken 4 days post-transfection. Nuclei are stained by Hoechst 33342 (cyan), cytoplasm is stained with Calcein (gray), and *ASCL1-gRNA* transfection is visualized by *mCherry* protein (yellow) expression. Scale bar = 50 μm. Enlarged (2×) images of the areas indicated by squares are included.

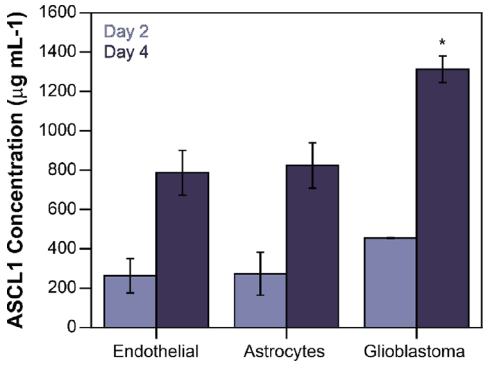

Figure 7. Intracellular concentration of ASCL1 protein mediated by RV-like NP transfection. Concentration of ASCL1 protein expressed in the different cell layers of the 3D BBB *in vitro* model measured by ELISA assay 2 and 4 days post-transfection. Error bars show the means ± standard deviation (n = 3). One-way ANOVA test was used to determine significant difference. *Significant difference found with respect to other cells from the corresponding day (p value < 0.05).

post-transfection with RV-like NPs. After performing statistical analysis using one-way ANOVA, we found that glioblastoma ASCL1 protein expression was significantly higher than in endothelial and astrocyte cells from the 3D BBB *in vitro* model.

3.6. Specific Recognition of RV-like NPs in the 3D BBB *In Vitro* Model. An important design component of RV-like NPs is the surface embedding of RVG29. This peptide is known to bind the nAchR and facilitate NP penetration across the BBB through the receptor-mediated transcytosis pathway.[66] Verifying that the 3D BBB *in vitro* model developed here expresses nAchR receptors is of utmost importance to understand RV-like NPs' cell translocation mechanism. We identified nAchR through immunochemistry using the recombinant anti-nicotinic acetylcholine receptor alpha 1/CHRNA1 antibody. First, we studied nAchR in endothelial, astrocyte, and glioblastoma cells cultured independently (Figure S7). Endothelial and glioblastoma cells showed no presence of nAchR, whereas astrocytes expressed nAchR. This observation was expected because it is known that astrocytes express multiple subunits of nAchR.[67,68] Then, the endothelial, astrocyte, and glioblastoma cell layers from the 3D BBB *in vitro* model were stained for the recombinant anti-nicotinic acetylcholine receptor alpha 1/CHRNA1 antibody (Figure 8), reveling the presence of nAchR receptors in all cell lines across the BBB *in vitro* model. We hypothesized that surface functionalization with RVG29 will endow specific biorecognition functions to the NPs for passaging the BBB. Specific biorecognition should occur between RVG29 and nAchR. Here, we showed that in our 3D BBB *in vitro* model, nAchR receptors are naturally formed when co-culturing the three cell lines. This has been previously shown and occurs to facilitate cell-to-cell communication within the co-cultures.[16,18]

3.7. Cytotoxicity of RV-like NPs. The cell viability of glioblastoma cells when using RV-like NPs as delivery carrier

https://doi.org/10.1021/acsanm.3c00651
ACS Appl. Nano Mater. 2023, 6, 6299−6311

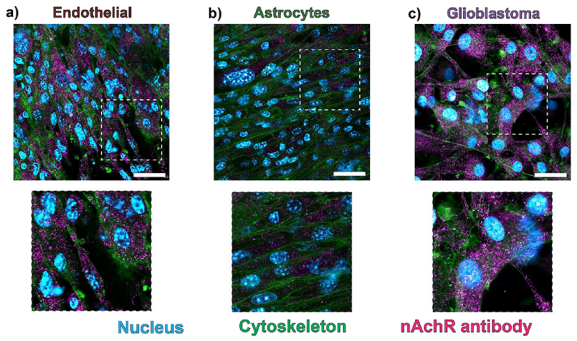

Figure 8. Expression of nAchR in the 3D BBB *in vitro* model. CLSM images of immunostaining for the recombinant anti-nicotinic acetylcholine receptor alpha 1/CHRNA1 antibody in (a) endothelial, (b) astrocyte, and (c) glioblastoma cells from the 3D BBB *in vitro* model. Nuclei are stained by DAPI (cyan), and the cytoskeleton is stained with Acti-stain 488 phalloidin (green) and nAchR antibody (magenta). Scale bar = 50 μm. Enlarged (2×) images of the areas indicated by squares are included.

of *ASCL1-gRNA* was investigated through the live/dead assay. Calcein and Sytox Red were used to label live and dead cells, respectively, to further quantify the cell populations using flow cytometry (Figure 9). Intact glioblastoma cells were used as the control group. Around 90 ± 0.8% of glioblastoma cells co-cultured with naked *ASCL1-gRNA*, empty PEG-PDHA NPs, or RV-like NPs were alive, whereas 10 ± 0.8% of the population was dead during the 4 days of co-culturing. The same percentages of live and dead cell populations are observed in intact glioblastoma cell cultures (control group), indicating no cytotoxic effects from the plasmid or from the NPs and rather 10.0 ± 0.8% of death in cells due to handling procedures such as detachment from the substrate with enzymes. When glioblastoma cells were transfected using Lipofectamine 3000, only 63.0 ± 0.8% of the cells were alive after 2 days of co-culturing, which is significantly lower than the control. After 4 days of exposure to Lipofectamine 3000, half of the cell population was dead. The detrimental effects of Lipofectamine on cells is expected because of the highly positive charge of the lipid-based carrier. The cytotoxicity of Lipofectamine 3000 has been previously reported utilizing various plasmids.[27,41,69,70]

4. CONCLUSIONS

In this work, we developed a nonviral platform for the intracellular delivery of gene editing tools across at BBB. A co-polymer from a poly(β amino ester), PEG-PDHA, was utilized to encapsulate *ASCL1-gRNA*. We previously demonstrated the potential of this polymer for gene therapy as it can be internalized by cells and translocate into their nucleus within a few hours of co-culturing. The surface of this nanoformulation was further engineered here to provide specific biorecognition functions for crossing the BBB and delivering the therapeutic cargo intracellularly. The surface engineering protocol followed mimicry of the surface chemistry of RV to form RV-like NPs. A 3D *in vitro* model of the BBB was established to evaluate the nanoformulation. RV-like NPs are capable of transiently crossing the 3D BBB *in vitro* model and internalizing into glioblastoma cells within 8 h of co-culturing. Once taken up by the cells, RV-like NPs dissociate as a result of polymer protonation at intracellular pH (<6), releasing the genetic material. RV-like NPs are preferentially internalized by glioblastoma cells from the 3D BBB *in vitro* model, transfecting them at a rate of 12% and causing no cytotoxicity. On the contrary, the Lipofectamine 3000 reagent is not efficient in crossing the 3D BBB *in vitro* model, transfecting primarily the contact endothelial cell layer of the model at a rate of 15%, and decreasing the viability of cells below 80%.

Mimicking the surface chemistry of rabies virus into synthetic nanocarriers by incorporating RVG29 enables a noninvasive strategy to transiently overcome the BBB. The surface functionalization approach presented here opens the possibility for new biomimicry approaches to overcome other challenging biological barriers. The developed nanoformulation has the potential to encapsulate and deliver other gene editing tools regardless of their size, a limiting factor in viral carriers. Further studies will explore *in vivo* gene delivery across the BBB for potential clinical translation. Understanding brain cellular pathways and the ability to engineer noninvasive routes across the BBB are expected to accelerate the development of new therapies for brain cancers and other brain diseases.

■ ASSOCIATED CONTENT

Supporting Information

The Supporting Information is available free of charge at https://pubs.acs.org/doi/10.1021/acsanm.3c00651.

TEM image of PEG-PDHA NPs; number and volume hydrodynamic size distributions for PEG-PDHA NPs and RV-like NPs; RVG29 assembly followed by QCM-D and FCS data; CLSM images following NP cell uptake at 4 and 12 h; transfection efficiency across the 3D BBB *in*

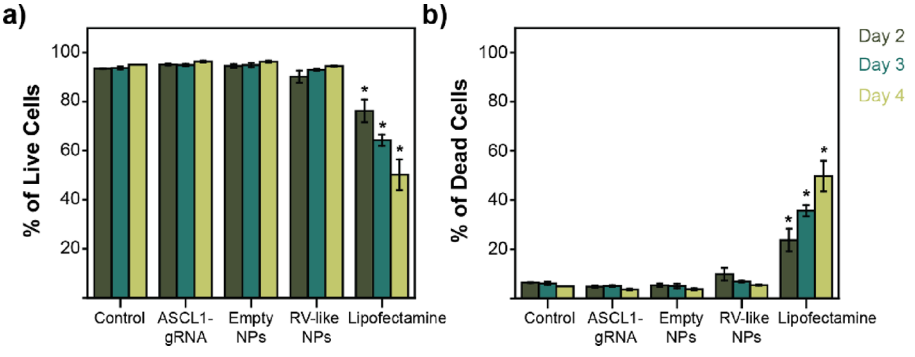

Figure 9. Cell viability. Percentage of (a) live and (b) dead cells from populations of 10,000 glioblastoma cells exposed to different conditions. Error bars show the means ± standard error of the mean (n = 3). One-way ANOVA test was used to determine significant difference. *Significant difference found with respect to the control (p value < 0.05).

https://doi.org/10.1021/acsanm.3c00651
ACS Appl. Nano Mater. 2023, 6, 6299−6311

vitro model at days 2 and 3 using Lipofectamine and RV-like NPs as carriers; and CLSM images showing nAchR expression on different cell lines cultured independently (PDF)

AUTHOR INFORMATION

Corresponding Author

Gabriela Romero − *Department of Biomedical Engineering and Chemical Engineering, The University of Texas at San Antonio, San Antonio, Texas 78249, United States;* orcid.org/0000-0001-8081-2946; Email: gabrielaromero.uribe@utsa.edu

Authors

Tina M. Rodgers − *Department of Biomedical Engineering and Chemical Engineering, The University of Texas at San Antonio, San Antonio, Texas 78249, United States*

Nicolas Muzzio − *Department of Biomedical Engineering and Chemical Engineering, The University of Texas at San Antonio, San Antonio, Texas 78249, United States*

Andrea Valero − *Department of Biomedical Engineering and Chemical Engineering, The University of Texas at San Antonio, San Antonio, Texas 78249, United States*

Ikram Ahmad − *Department of Biomedical Engineering and Chemical Engineering, The University of Texas at San Antonio, San Antonio, Texas 78249, United States*

Tanja Ursula Lüdtke − *Soft Matter Nanotechnology, CIC biomaGUNE, Basque Research and Technology Alliance (BRTA), San Sebastian, Gipuzkoa 20014, Spain*

Sergio E. Moya − *Soft Matter Nanotechnology, CIC biomaGUNE, Basque Research and Technology Alliance (BRTA), San Sebastian, Gipuzkoa 20014, Spain;* orcid.org/0000-0002-7174-1960

Complete contact information is available at: https://pubs.acs.org/10.1021/acsanm.3c00651

Author Contributions

The manuscript was written through contributions of all authors. All authors have given approval to the final version of the manuscript.

Funding

This work was supported partially by the National Science Foundation under a CAREER award to Gabriela Romero (CBET-2044713).

Notes

The authors declare no competing financial interest.

ABBREVIATIONS

ASCL1-gRNA, achaete-scute family bHLH transcription factor 1 CRISPR guide RNA
BBB, blood−brain barrier
RV, rabies virus
RVG, rabies virus glycoprotein
RVG29, 29-residue peptide derived from RVG
RV-like NPs, nanoparticles with RVG29
CLSM, confocal laser scanning microscope
GBM, glioblastoma multiforme
nAchR, nicotinic acetylcholine receptor
siRNA, small interfering RNAs
ZFN, zinc finger nucleases
TALENS, transcription activator-like effector nucleases
CRISPR/Cas9, clustered regularly interspaced short palindromic repeats
NPs, nanoparticles
PEG-PDHA, poly(ethylene glycol)-*block*-poly(1,4-butanediol)-diacrylate-*β*-hydroxyamylamine-*block*-poly(ethylene glycol)
MTAS-NLS, microtubule associated nuclear localization peptide
RhB, Rhodamine B
DMSO, dimethyl sulfoxide
TEA, triethylamine
Py, pyridine
NaCl, sodium chloride
PEI, poly(ethylenimine)
NaOH, sodium hydroxide
HCl, hydrochloric acid
DAPI, 4′,6-diamidino-2-phenylindole
EDC, (1-ethyl-3-(3-dimethylaminopropyl)carbodiimide hydrochloride
NHS, hydroxysuccinimide
MTT, 3-(4,5-dimethylthiazol-2-yl)-2,5-diphynyltetrazolium bromide
PBS, phosphate buffer saline
FBS, fetal bovine serum
EBM, endothelial cell growth basal medium
DMEM, Dulbecco's modified Eagle medium
EMEM, Eagle's minimum essential medium
QCM-D, quartz crystal microbalance with dissipation
HUVEC, human primary umbilical vein endothelial cell line
U87MG, Uppsala 87 malignant glioma cell line
C8-D1A, immortal mouse clone type I neuronal astrocyte cell line
TEER, transendothelial electrical resistance
ELISA, enzyme-linked immunosorbent assay
TEM, transmission electron microscopy
DLS, dynamic light scattering
FCS, fluorescence correlation spectroscopy

REFERENCES

(1) Guan, X.; Hasan, M. N.; Maniar, S.; Jia, W.; Sun, D. Reactive Astrocytes in Glioblastoma Multiforme. *Mol. Neurobiol.* **2018**, *55*, 6927−6938.

(2) Carlsson, S. K.; Brothers, S. P.; Wahlestedt, C. Emerging treatment strategies for glioblastoma multiforme. *EMBO Mol. Med.* **2014**, *6*, 1359−1370.

(3) Davis, M. E. Glioblastoma: Overview of Disease and Treatment. *Clin. J. Oncol. Nurs.* **2016**, *20*, S2−S8.

(4) Price, R. L.; Chiocca, E. A. Evolution of malignant glioma treatment: from chemotherapy to vaccines to viruses. *Neurosurgery* **2014**, *61*, 74−83.

(5) Zhang, Z. X.; Chen, J. X.; Shi, B. Z.; Li, G. H.; Li, Y.; Xiang, Y.; Qin, X.; Yang, L.; Lv, S. Q. Multifocal glioblastoma-two case reports and literature review. *Chin. Neurosurg. J.* **2021**, *7*, 8.

(6) Rivera, M.; Sukhdeo, K.; Yu, J. Ionizing radiation in glioblastoma initiating cells. *Front. Oncol.* **2013**, *3*, 74.

(7) Ballabh, P.; Braun, A.; Nedergaard, M. The blood-brain barrier: an overview: structure, regulation, and clinical implications. *Neurobiol. Dis.* **2004**, *16*, 1−13.

(8) Shergalis, A.; Bankhead, A., 3rd; Luesakul, U.; Muangsin, N.; Neamati, N. Current Challenges and Opportunities in Treating Glioblastoma. *Pharmacol. Rev.* **2018**, *70*, 412−445.

(9) Furtado, D.; Bjornmalm, M.; Ayton, S.; Bush, A. I.; Kempe, K.; Caruso, F. Overcoming the Blood-Brain Barrier: The Role of Nanomaterials in Treating Neurological Diseases. *Adv. Mater.* **2018**, *30*, No. e1801362.

(10) Upadhyay, R. K. Drug delivery systems, CNS protection, and the blood brain barrier. *BioMed Res. Int.* **2014**, *2014*, 869269.
(11) Zhou, Y.; Peng, Z.; Seven, E. S.; Leblanc, R. M. Crossing the blood-brain barrier with nanoparticles. *J. Controlled Release* **2018**, *270*, 290−303.
(12) He, Q.; Liu, J.; Liang, J.; Liu, X.; Li, W.; Liu, Z.; Ding, Z.; Tuo, D. Towards Improvements for Penetrating the Blood-Brain Barrier-Recent Progress from a Material and Pharmaceutical Perspective. *Cell* **2018**, *7*, 24.
(13) Gumerlock, M. K.; Belshe, B. D.; Madsen, R.; Watts, C. Osmotic blood-brain barrier disruption and chemotherapy in the treatment of high grade malignant glioma: patient series and literature review. *J. Neuro-Oncol.* **1992**, *12*, 33−46.
(14) Teichberg, V. I. From the liver to the brain across the blood-brain barrier. *Proc. Natl. Acad. Sci. U. S. A.* **2007**, *104*, 7315−7316.
(15) Pardridge, W. M. The blood-brain barrier: bottleneck in brain drug development. *NeuroRx* **2005**, *2*, 3−14.
(16) Lee, C.; Hwang, H. S.; Lee, S.; Kim, B.; Kim, J. O.; Oh, K. T.; Lee, E. S.; Choi, H. G.; Youn, Y. S. Rabies Virus-Inspired Silica-Coated Gold Nanorods as a Photothermal Therapeutic Platform for Treating Brain Tumors. *Adv. Mater.* **2017**, *29*, 1605563.
(17) Tang, L.; Feng, Y.; Gao, S.; Mu, Q.; Liu, C. Nanotherapeutics Overcoming the Blood-Brain Barrier for Glioblastoma Treatment. *Front. Pharmacol.* **2021**, *12*, No. 786700.
(18) Huey, R.; Hawthorne, S.; McCarron, P. The potential use of rabies virus glycoprotein-derived peptides to facilitate drug delivery into the central nervous system: a mini review. *J. Drug Targeting* **2017**, *25*, 379−385.
(19) Oller-Salvia, B.; Sanchez-Navarro, M.; Giralt, E.; Teixido, M. Blood-brain barrier shuttle peptides: an emerging paradigm for brain delivery. *Chem. Soc. Rev.* **2016**, *45*, 4690−4707.
(20) Hajj, K. A.; Whitehead, K. A. Tools for translation: non-viral materials for therapeutic mRNA delivery. *Nat. Rev. Mater.* **2017**, *2*, 17056.
(21) Wittrup, A.; Lieberman, J. Knocking down disease: a progress report on siRNA therapeutics. *Nat. Rev. Genet.* **2015**, *16*, 543−552.
(22) Glass, Z.; Lee, M.; Li, Y.; Xu, Q. Engineering the Delivery System for CRISPR-Based Genome Editing. *Trends Biotechnol.* **2018**, *36*, 173−185.
(23) Gaj, T.; Gersbach, C. A.; Barbas, C. F., 3rd ZFN, TALEN, and CRISPR/Cas-based methods for genome engineering. *Trends Biotechnol.* **2013**, *31*, 397−405.
(24) Nemudryi, A. A.; Valetdinova, K. R.; Medvedev, S. P.; Zakian, S. M. TALEN and CRISPR/Cas Genome Editing Systems: Tools of Discovery. *Acta Naturae* **2014**, *6*, 19−40.
(25) Gilbert, L. A.; Larson, M. H.; Morsut, L.; Liu, Z.; Brar, G. A.; Torres, S. E.; Stern-Ginossar, N.; Brandman, O.; Whitehead, E. H.; Doudna, J. A.; Lim, W. A.; Weissman, J. S.; Qi, L. S. CRISPR-mediated modular RNA-guided regulation of transcription in eukaryotes. *Cell* **2013**, *154*, 442−451.
(26) Woltjen, K.; Michael, I. P.; Mohseni, P.; Desai, R.; Mileikovsky, M.; Hamalainen, R.; Cowling, R.; Wang, W.; Liu, P.; Gertsenstein, M.; Kaji, K.; Sung, H. K.; Nagy, A. piggyBac transposition reprograms fibroblasts to induced pluripotent stem cells. *Nature* **2009**, *458*, 766−770.
(27) Rodgers, T.; Muzzio, N.; Watson, C.; Romero, G. Stabilization of Poly (beta-Amino Ester) Nanoparticles for the Efficient Intracellular Delivery of PiggyBac Transposon. *Bioengineering* **2021**, *8*, 16.
(28) Rathnam, C.; Chueng, S. D.; Yang, L.; Lee, K. B. Advanced Gene Manipulation Methods for Stem Cell Theranostics. *Theranostics* **2017**, *7*, 2775−2793.
(29) Tang, B. L. The Potential of Targeting Brain Pathology with Ascl1/Mash1. *Cell* **2017**, *6*, 26.
(30) Cheng, X.; Tan, Z.; Huang, X.; Yuan, Y.; Qin, S.; Gu, Y.; Wang, D.; He, C.; Su, Z. Inhibition of Glioma Development by ASCL1-Mediated Direct Neuronal Reprogramming. *Cell* **2019**, *8*, 571.
(31) Guillemot, F.; Hassan, B. A. Beyond proneural: emerging functions and regulations of proneural proteins. *Curr. Opin. Neurobiol.* **2017**, *42*, 93−101.
(32) Park, N. I.; Guilhamon, P.; Desai, K.; McAdam, R. F.; Langille, E.; O'Connor, M.; Lan, X.; Whetstone, H.; Coutinho, F. J.; Vanner, R. J.; Ling, E.; Prinos, P.; Lee, L.; Selvadurai, H.; Atwal, G.; Kushida, M.; Clarke, I. D.; Voisin, V.; Cusimano, M. D.; Bernstein, M.; Das, S.; Bader, G.; Arrowsmith, C. H.; Angers, S.; Huang, X.; Lupien, M.; Dirks, P. B. ASCL1 Reorganizes Chromatin to Direct Neuronal Fate and Suppress Tumorigenicity of Glioblastoma Stem Cells. *Cell Stem Cell* **2017**, *21*, 209−224.e7.
(33) Uddin, F.; Rudin, C. M.; Sen, T. CRISPR Gene Therapy: Applications, Limitations, and Implications for the Future. *Front. Oncol.* **2020**, *10*, 1387.
(34) Naso, M. F.; Tomkowicz, B.; Perry, W. L., 3rd; Strohl, W. R. Adeno-Associated Virus (AAV) as a Vector for Gene Therapy. *BioDrugs* **2017**, *31*, 317−334.
(35) Fus-Kujawa, A.; Prus, P.; Bajdak-Rusinek, K.; Teper, P.; Gawron, K.; Kowalczuk, A.; Sieron, A. L. An Overview of Methods and Tools for Transfection of Eukaryotic Cells in vitro. *Front. Bioeng. Biotechnol.* **2021**, *9*, No. 701031.
(36) Potter, H. Transfection by electroporation. *Curr. Protoc. Mol. Biol.* **2003**, *121*, 9−3.
(37) Berardo, C.; Siciliano, V.; Di Pasqua, L. G.; Richelmi, P.; Vairetti, M.; Ferrigno, A. Comparison between Lipofectamine RNAiMAX and GenMute transfection agents in two cellular models of human hepatoma. *Eur. J. Histochem.* **2019**, *63*, 3048.
(38) Cardarelli, F.; Digiacomo, L.; Marchini, C.; Amici, A.; Salomone, F.; Fiume, G.; Rossetta, A.; Gratton, E.; Pozzi, D.; Caracciolo, G. The intracellular trafficking mechanism of Lipofectamine-based transfection reagents and its implication for gene delivery. *Sci. Rep.* **2016**, *6*, 25879.
(39) Rao, S.; Morales, A. A.; Pearse, D. D. The Comparative Utility of Viromer RED and Lipofectamine for Transient Gene Introduction into Glial Cells. *BioMed Res. Int.* **2015**, *2015*, No. 458624.
(40) Clements, B. A.; Incani, V.; Kucharski, C.; Lavasanifar, A.; Ritchie, B.; Uludag, H. A comparative evaluation of poly-L-lysine-palmitic acid and Lipofectamine 2000 for plasmid delivery to bone marrow stromal cells. *Biomaterials* **2007**, *28*, 4693−4704.
(41) San Juan, A. M. T.; Rodgers, T.; Bedolla, C.; Noriega, F.; Romero, G. Layer by layer surface engineering of poly(lactide-co-glycolide)nanoparticles for plasmid DNA delivery. *J. Appl. Polym. Sci.* **2020**, *137*, 49377.
(42) Rodgers, T. M. Engineering Biomimetic Carriers as Gene Editing Platforms for Treating Brain Tumors. Ph.D., The University of Texas at San Antonio, United States -- Texas, 2022.
(43) Ramos, J. I.; Moya, S. E. Effect of the Density of ATRP Thiol Initiators in the Yield and Water Content of Grafted-From PMETAC Brushes. A Study by Means of QCM-D and Spectroscopic Ellipsometry Combined in a Single Device. *Macromol. Chem. Phys.* **2012**, *213*, 549−556.
(44) Sauerbrey, G. Verwendung Von Schwingquarzen Zur Wagung Dunner Schichten Und Zur Mikrowagung. *Z. Phys.* **1959**, *155*, 206−222.
(45) Reviakine, I.; Johannsmann, D.; Richter, R. P. Hearing what you cannot see and visualizing what you hear: interpreting quartz crystal microbalance data from solvated interfaces. *Anal. Chem.* **2011**, *83*, 8838−8848.
(46) Stone, N. L.; England, T. J.; O'Sullivan, S. E. A Novel Transwell Blood Brain Barrier Model Using Primary Human Cells. *Front. Cell Neurosci.* **2019**, *13*, 230.
(47) Mc Carthy, D. J.; Malhotra, M.; O'Mahony, A. M.; Cryan, J. F.; O'Driscoll, C. M. Nanoparticles and the blood-brain barrier: advancing from in-vitro models towards therapeutic significance. *Pharm. Res.* **2015**, *32*, 1161−1185.
(48) Swamy, T.; Raviteja, P.; Subba Reddy, B. V.; Ravinder, V. Efficient Method for the Synthesis of Benzamides from Benzoic Acids and Aryl Isothiocyanates using K2HPO4. *ChemistrySelect* **2017**, *2*, 7612−7614.
(49) Chen, S.; Einspanier, R.; Schoen, J. Transepithelial electrical resistance (TEER): a functional parameter to monitor the quality of

https://doi.org/10.1021/acsanm.3c00651
ACS Appl. Nano Mater. 2023, 6, 6299−6311

oviduct epithelial cells cultured on filter supports. *Histochem. Cell Biol.* **2015**, *144*, 509−515.
(50) Bhattacharjee, S. DLS and zeta potential − What they are and what they are not? *J. Controlled Release* **2016**, *235*, 337−351.
(51) Souza, T. G. F.; Ciminelli, V. S. T.; Mohallem, N. D. S. A comparison of TEM and DLS methods to characterize size distribution of ceramic nanoparticles. *J. Phys.: Conf. Ser.* **2016**, *733*, No. 012039.
(52) Hoo, C. M.; Starostin, N.; West, P.; Mecartney, M. L. A comparison of atomic force microscopy (AFM) and dynamic light scattering (DLS) methods to characterize nanoparticle size distributions. *J. Nanopart. Res.* **2008**, *10*, 89−96.
(53) Tang, S.; Yin, Q.; Su, J.; Sun, H.; Meng, Q.; Chen, Y.; Chen, L.; Huang, Y.; Gu, W.; Xu, M.; Yu, H.; Zhang, Z.; Li, Y. Inhibition of metastasis and growth of breast cancer by pH-sensitive poly (beta-amino ester) nanoparticles co-delivering two siRNA and paclitaxel. *Biomaterials* **2015**, *48*, 1−15.
(54) Tang, S.; Meng, Q.; Sun, H.; Su, J.; Yin, Q.; Zhang, Z.; Yu, H.; Chen, L.; Gu, W.; Li, Y. Dual pH-sensitive micelles with charge-switch for controlling cellular uptake and drug release to treat metastatic breast cancer. *Biomaterials* **2017**, *114*, 44−53.
(55) Iqbal, S.; Zhao, Z. Poly (beta amino esters) copolymers: Novel potential vectors for delivery of genes and related therapeutics. *Int. J. Pharm.* **2022**, *611*, No. 121289.
(56) Appelt-Menzel, A.; Cubukova, A.; Gunther, K.; Edenhofer, F.; Piontek, J.; Krause, G.; Stuber, T.; Walles, H.; Neuhaus, W.; Metzger, M. Establishment of a Human Blood-Brain Barrier Co-culture Model Mimicking the Neurovascular Unit Using Induced Pluri- and Multipotent Stem Cells. *Stem Cell Rep.* **2017**, *8*, 894−906.
(57) Shayan, G.; Choi, Y. S.; Shusta, E. V.; Shuler, M. L.; Lee, K. H. Murine in vitro model of the blood-brain barrier for evaluating drug transport. *Eur. J. Pharm. Sci.* **2011**, *42*, 148−155.
(58) Hind, W. H.; Tufarelli, C.; Neophytou, M.; Anderson, S. I.; England, T. J.; O'Sullivan, S. E. Endocannabinoids modulate human blood-brain barrier permeability in vitro. *Br. J. Pharmacol.* **2015**, *172*, 3015−3027.
(59) Nikandish, N.; Hosseinzadeh, L.; Hemati Azandaryani, A.; Derakhshandeh, K. The Role of Nanoparticle in Brain Permeability: An in-vitro BBB Model. *Iran. J. Pharm. Res.* **2016**, *15*, 403−413.
(60) Yin, W.; Xiang, P.; Li, Q. Investigations of the effect of DNA size in transient transfection assay using dual luciferase system. *Anal. Biochem.* **2005**, *346*, 289−294.
(61) Campeau, P.; Chapdelaine, P.; Seigneurin-Venin, S.; Massie, B.; Tremblay, J. P. Transfection of large plasmids in primary human myoblasts. *Gene Ther.* **2001**, *8*, 1387−1394.
(62) Cherng, J. Y.; van de Wetering, P.; Talsma, H.; Crommelin, D. J.; Hennink, W. E. Effect of size and serum proteins on transfection efficiency of poly ((2-dimethylamino)ethyl methacrylate)-plasmid nanoparticles. *Pharm. Res.* **1996**, *13*, 1038−1042.
(63) Botto, C.; Dalkara, D.; El-Amraoui, A. Progress in Gene Editing Tools and Their Potential for Correcting Mutations Underlying Hearing and Vision Loss. *Front. Genom. Ed.* **2021**, *3*, No. 737632.
(64) Kim, K.; Park, S. W.; Kim, J. H.; Lee, S. H.; Kim, D.; Koo, T.; Kim, K. E.; Kim, J. H.; Kim, J. S. Genome surgery using Cas9 ribonucleoproteins for the treatment of age-related macular degeneration. *Genome Res.* **2017**, *27*, 419−426.
(65) Holmgaard, A. B.; Askou, A. L.; Jensen, E. G.; Alsing, S.; Bak, R. O.; Mikkelsen, J. G.; Corydon, T. J. Targeted Knockout of the Vegfa Gene in the Retina by Subretinal Injection of RNP Complexes Containing Cas9 Protein and Modified sgRNAs. *Mol. Ther.* **2021**, *29*, 191−207.
(66) Fu, C.; Xiang, Y.; Li, X.; Fu, A. Targeted transport of nanocarriers into brain for theranosis with rabies virus glycoprotein-derived peptide. *Mater. Sci. Eng.* **2018**, *87*, 155−166.
(67) Teaktong, T.; Graham, A. J.; Court, J. A.; Perry, R. H.; Jaros, E.; Johnson, M.; Hall, R.; Perry, E. K. Nicotinic acetylcholine receptor immunohistochemistry in Alzheimer's disease and dementia with Lewy bodies: differential neuronal and astroglial pathology. *J. Neurol. Sci.* **2004**, *225*, 39−49.
(68) Mitra, S.; Khatri, S. N.; Maulik, M.; Bult-Ito, A.; Schulte, M. Allosterism of Nicotinic Acetylcholine Receptors: Therapeutic Potential for Neuroinflammation Underlying Brain Trauma and Degenerative Disorders. *Int. J. Mol. Sci.* **2020**, *21*, 4918.
(69) Wang, T.; Larcher, L. M.; Ma, L.; Veedu, R. N. Systematic Screening of Commonly Used Commercial Transfection Reagents towards Efficient Transfection of Single-Stranded Oligonucleotides. *Molecules* **2018**, *23*, 2564.
(70) Rahimi, P.; Mobarakeh, V. I.; Kamalzare, S.; SajadianFard, F.; Vahabpour, R.; Zabihollahi, R. Comparison of transfection efficiency of polymer-based and lipid-based transfection reagents. *Bratisl. Lek. Listy* **2018**, *119*, 701−705.

https://doi.org/10.1021/acsanm.3c00651
ACS Appl. Nano Mater. 2023, 6, 6299−6311